

Transient Emission From Dissipative Fronts in Magnetized, Relativistic Outflows. II. Synchrotron Flares

Amir Levinson

School of Physics and Astronomy, Tel Aviv University, Tel Aviv 69978, Israel

ABSTRACT

The time dependent synchrotron emission from relativistic jets, and the relation between the synchrotron and ERC emission is considered within the framework of the radiative front model. The timescale and profile of the optically thin emission are shown to be determined, in this model, by the shock formation radius, the thickness of expelled fluid slab and the variation of the front's parameters due to its transverse expansion. For a range of reasonable conditions, a variety of flare shapes can be produced, varying from roughly symmetric with exponential rises and decays, as often seen in blazars, to highly asymmetric with a fast rise and a much slower, power law decay, as seen in GRB afterglows. The onset, duration, and fluence of low-frequency (below the initial turnover frequency) and hard gamma-ray (above the initial gamma-spheric energy) outbursts are limited by opacity effects; the emission at these energies is quite generally delayed and, in the case of sufficiently short length outbursts, severely attenuated. The observational consequences are discussed. One distinctive prediction of this model is that in a single, powerful source, the upper cutoff of the gamma-ray spectrum should be correlated with the timescale of the outburst and with the amplitude of variations at long wavelengths (typically radio to millimeter).

1. Introduction

It is widely believed that the rapid variability frequently observed in blazars (for reviews see Ulrich, et al. 1997; Wagner, 1997) is linked to dissipation in relativistic jets. The characteristically short variability time scales - down to a few minutes at optical and x-ray wavelengths (e.g., Wagner 1997), and several hours at gamma-ray energies (Mattox, J., et al. 1997; Aharonian et al. 1998) - indicate that the source is compact and strongly beamed, supporting this view. Despite the apparent complexity of the temporal behavior exhibited by blazars, ongoing observational efforts have revealed some trends. Firstly, the high-and low-energy emission appears to be well correlated. Correlations between optical/UV and gamma-ray emission have been observed in many blazars (Wagner, 1997, and references therein), and between the X-ray and TeV emission in the TeV BL Lac objects (Macomb et al. 1995; Buckley et al. 1996; Aharonian et al. 1998). There is also evidence for a correlated activity at radio and gamma-ray bands in some cases (e.g., 3C279; Wehrle et al. 1998). Secondly, the variation of the synchrotron emission below the spectral turnover has the tendency to be slower and later at longer wavelengths (with the exception of radio IDV), suggesting that the low frequency (radio-to-IR) emission is self-absorbed at the early stages of the outburst. In spite of these trends, it seems that blazars can exhibit a variety of temporal behaviors, and that even in individual sources the variability pattern can change, as exemplified by observations of the BL Lac object PKS 2155-304 that revealed different variability patterns during the 1991 (e.g., Brinkmann et al. 1994; Edelson et al. 1995) and 1994 (Urry et al. 1997) campaigns. The change in temporal behavior can be ascribed to the different physical conditions that exist in the source during each episode, and it is, therefore, desirable

to examine the dependence of the temporal characteristics of the emission on the physical parameters of the source.

In this paper we study the time dependent synchrotron emission from relativistic jets in the framework of the radiative front model developed previously to study gamma-ray flares (Levinson, 1998; hereafter Paper I). The model is extended to encompass synchrotron emission and employed to calculate the temporal evolution of the synchrotron and ERC emission radiated by the front, with an attempt to elucidate the dependence of the variability pattern on the model parameters. As shown below, the model can successfully account for some of the trends mentioned above, and predicts some additional features. In §2 we give an outline of the model and the necessary extensions. In §3 we derive the equation governing the evolution of the synchrotron flux in the front, and explain how it is incorporated into the numerical model. We then go on to describe the numerical results. The observational consequences are discussed in §4.

2. Description of the model

The model presented in Paper I assumes that the variable emission seen in blazars originates inside dissipative fronts that are produced by overtaking collisions of highly magnetized, relativistic outflows, and consists of a pair of shocks and a contact discontinuity (Romanova & Lovelace, 1997; Levinson & Van Putten, 1997). The front propagates with a velocity intermediate between that of the slow and fast fluid slabs, dissipates a fraction of the outflow energy, and cools radiatively and adiabatically. A fraction of the dissipation power is tapped for the acceleration of electrons to high energies, and the rest for the heating of the bulk plasma in the front. The acceleration time of non-thermal electrons has been assumed to be short compared with the cooling and the corresponding light crossing times. Further, the fluid parameters and the fraction of dissipation power that is tapped for electron acceleration are assumed to have no explicit time dependence (but do depend on time implicitly through the dynamics of the front). As a consequence, the characteristics of the transient emission produced by this model reflect essentially the dynamics of the system, as well as the intensity of external radiation, rather than explicit variations of the outflow parameters and/or electron acceleration rate, as, e.g., in the one-zone, homogeneous model by Mastichiadis & Kirk (1997).

In Paper I we focused on the production of gamma-ray flares in the regime where ERC emission (e.g., Dermer & Schlickheiser 1993; Blandford & Levinson 1995) dominates over SSC emission (Bloom & Marscher 1993). The dynamics of the system and the time evolution of the flux radiated by the front have been calculated in a self-consistent manner, by numerically solving the MHD equations governing the front structure coupled to the kinetic equations describing the angle averaged pair and gamma-ray distribution functions. The solutions depend on four key parameters: i) the dissipation rate of magnetic energy, ii) the maximum injection energy of electrons, denoted by E_{emax} , which was taken to be fixed in the observer frame for simplicity, iii) the fraction of dissipation energy that is injected in the form of non-thermal electrons, and iv) the ratio of the thickness of ejected fluid slab and the gradient length scale of background radiation intensity. The latter parameter determines essentially whether the shape and timescale of the flare are related to the radial variation of ambient radiation intensity, in which case the light curve is asymmetric with a rapid rise and a longer decay, or to the shock travel time across the fast fluid slab, in which case the decay time is of order the cooling time and is typically much shorter than in the case of infinite length outbursts. As shown in Paper I, the temporal evolution of the gamma-ray flux is insensitive to the injected electron spectrum provided that electron acceleration is efficient, and that E_{emax} exceeds the corresponding gamma-spheric energy at any given radius along the course of the front. The evolution

of the synchrotron spectrum, on the other hand, is expected to depend on variations of E_{emax} , particularly if the front is optically thin at the corresponding frequencies (cf. Levinson 1996). We shall, therefore, relax the assumption that E_{emax} is fixed. In general, the evolution of the injected electron distribution is governed by the acceleration process, and a self-consistent treatment of particle acceleration is required in order to follow the development of E_{emax} . Such a treatment is beyond the scope of our paper. Here we settle for a simple prescription where the injected spectrum is taken to be a power law with an exponential cutoff above $E_{emax}(t)$, where

$$E_{emax}(t) = E_o(r/r_o)^b, \quad (1)$$

with $r(t) = r_o + \beta_c ct$.

One important feature of the model is a positive radiative feedback that affects the emitted spectrum considerably. The point is that as a result of radiative losses the front decelerates and its expansion rate decreases until the peak of the radiated power is reached. The deceleration of the front leads, in turn, to enhanced dissipation rate of the bulk flow energy, since the relative velocity between the fast fluid and the reverse shock increases. After peak emission is reached, the front begins to reaccelerate, ultimately reaching its initial speed and structure. The consequences of this radiative feedback for the variability have been discussed in detail in Paper I. Another consequence is that the variability should depend strongly on the orientation of the source, owing to the change in beaming factor during the deceleration phase. The analysis presented in Paper I cannot account for such orientation effects, as it only treats the angle averaged flux. The model does describe rather well, however, the variability that would be seen by an observer at sufficiently small viewing angle. A study of orientation effects will be presented elsewhere (Eldar & Levinson, in preparation).

3. Synchrotron flares

In this section we extend the analysis to incorporate synchrotron emission, and apply the results to study the relation between the low-and high-energy emission in ERC dominated blazars. In order to do so, we augment the set of equations introduced in Paper I by an equation governing the time change of the synchrotron intensity (see eq. [3] below). We also include additional loss term for the electrons accounting for synchrotron cooling. The equations are then integrated in the injection frame (the rest frame of the boundary from which the fluid is expelled), as described in Paper I. Now, the synchrotron opacity depends on the electron density and magnetic field inside the front and, consequently, on the transverse expansion of the front. Let $c_{s\perp}$ denotes the expansion speed in the transverse direction, d the cross-sectional radius, and $A = \pi d^2$ the cross-sectional area. The expansion speed $c_{s\perp}$ may depend on external pressure and magnetic fields, or the density of ambient gas if inertial effects are important, and should not be the same as the sound speed in the radial direction in general. We suppose that initially $d_o = \psi r_o$, where ψ is the jet opening angle, and r_o is the radius of formation of the front (Paper I). Then $d = d_o + c_{s\perp} t = \psi[r_o + (c_{s\perp}/\psi)t]$. For illustration we take $(c_{s\perp}/\psi)$ to be equal to the front velocity, $c\beta_c$. We then obtain $A(t) \propto r^2(t)$, where $r(t) = (r_o + c\beta_c t)$. Let N_e be the total number of electrons in the front. The corresponding number density is then given by $n_e = N_e/(\Delta X A)$, where ΔX is the axial length of the front. The magnetic field is assumed to decline like

$$B = B_o[r(t)/r_o]^{-p}. \quad (2)$$

3.1. Transfer equation

We define $I_\nu(t, \mu)$ to be the unpolarized synchrotron intensity inside the front, as measured in the injection frame. The equation governing the time evolution of I_ν can be derived in the manner described in Paper I. One then obtains,

$$\frac{\partial}{\partial x^0} I_\nu = j - [(\mu - \beta_{s-})/(\Delta X) + \kappa] I_\nu, \quad (3)$$

where $j(\nu, \mu, t)$ and $\kappa(\nu, \mu, t)$ are the emission and absorption coefficients, $x^0 = ct$, β_{s-} is the velocity of the reverse shock, $\cos^{-1} \mu$ is the angle between the direction of a photon and the front velocity, and ΔX is the axial length of the front. The term proportional to $(\mu - \beta_{s-})$ accounts for the change in the intensity due to the combined effects of front expansion and escape of synchrotron photons from the front (see Paper I for details). For convenience, we compute the emission and absorption coefficients in the rest frame of the front (quantities measured in the front frame are henceforth denoted by prime), and then transform them to the injection frame. The coefficients in the two frames are related through (Rybicki & Lightman 1979),

$$j(\nu, \mu) = \left(\frac{\nu}{\nu'}\right)^2 j'(\nu', \mu'), \quad (4)$$

$$\kappa(\nu, \mu) = \frac{\nu'}{\nu} \kappa'(\nu', \mu'), \quad (5)$$

with $\nu = \mathcal{D}\nu'$, $\mathcal{D} = [\Gamma_c(1 - \beta_c\mu)]^{-1}$ being the Doppler factor, where Γ_c is the bulk Lorentz factor of the front. The emission and absorption coefficients are given in the front frame by,

$$j' = \frac{\sqrt{3}e^3}{4\pi mc^2} B(t) \sin \phi' \int n'_e(\mathcal{E}', t) F(x') d\mathcal{E}', \quad (6)$$

$$\kappa' = \frac{\sqrt{3}e^3}{8\pi m\nu'^2} B(t) \sin \phi' \int \mathcal{E}'^2 \frac{d}{d\mathcal{E}'} \left[\frac{n'_e}{\mathcal{E}'^2} \right] F(x') d\mathcal{E}'. \quad (7)$$

Here \mathcal{E}' is the electron energy with respect to the front frame, n'_e is the corresponding electron number density per unit energy, ϕ' is the angle between the line of sight and the magnetic field in the front frame, $x' = \nu'/\nu'_c$; $\nu'_c = (3e/4\pi mc)B(t) \sin \phi' (\mathcal{E}'/mc^2)^2$, and $F(x) = x \int_x^\infty K_{5/3}(\chi) d\chi$. We emphasize that $B(t)$, $\Gamma_c(t)$, and $\beta_{s-}(t)$ are not given explicitly but rather calculated self-consistently by integrating the front equations. Now, as mentioned above, the integration of the electron kinetic equation is carried out in the injection frame. This yields $n_e(t, \mathcal{E})$. Thus, in order to obtain $n'_e(t, \mathcal{E}')$ we need to transform n_e into the front frame. The appropriate transformation is derived in the Appendix under the assumption that the comoving electron distribution is isotropic.

As a check on the above equation, consider the case of a radiating blob, for which $\beta_{s+} = \beta_{s-} = \beta_c$. It can be readily shown that the steady-state solution of eq. (3) reduces, in the optically thin limit, to $I = j\Delta X/(\mu - \beta_c)$. On substituting $\Delta X' = \Gamma_c \Delta X$ and $\mu' = (\mu - \beta_c)/(1 - \beta_c\mu)$ in the latter expression, we recover the well known result: $I = \mathcal{D}^3(j'\Delta X'/\mu') = \mathcal{D}^3 I'$. Note that $\Delta X'$ and μ' are respectively the blob thickness and the cosine of the angle between the blob velocity and the direction of a photon, as measured in the blob frame.

We shall proceed by assuming that the magnetic field in the front is tangled and has no net direction. The emission and absorption coefficients can then be averaged over ϕ' . Since we do not consider polarization and orientation effects, we anticipate the results not to depend strongly on this assumption. We further average eq. (3) over the viewing angle μ .

3.2. Cooling rates

The synchrotron cooling time can be expressed in terms of the front parameters as

$$\frac{ct_{syn}}{r_o} = 0.17 \left(\frac{L_{j46}}{r_{o16}} \right)^{-1} \Gamma_{A-}^2 (n_f/n_-) U_{Af}^2 (\mathcal{E}/mc^2)^{-1}. \quad (8)$$

Here n_f , n_- are the electron densities inside the front and in the fluid exterior to the front, respectively, U_{Af} is the Alfvén 4-velocity with respect to front frame, L_{j46} is the power carried by the fast outflow in units of 10^{46} erg s $^{-1}$, Γ_{A-} is the Lorentz factor associated with the Alfvén 4-velocity of the exterior fluid, and r_{o16} is the radius of shock formation r_o in units of 10^{16} cm. For magnetized jets $\Gamma_{A-} \gg 1$. The product $(n_f/n_-)U_{Af}$ changes with time due to the radiative feedback (Paper I), and is typically of order 30 or so in the presence of rapid magnetic field dissipation. Thus, the synchrotron cooling time at most electron energies is much shorter than the dynamical time r_o/c . The ratio of synchrotron and Compton cooling rates equals the ratio of comoving energy densities of magnetic field and external radiation field, and is given by

$$\frac{t_{IC}}{t_{syn}} \simeq \frac{20}{\Gamma_{A-}^2 \Gamma_c^2} \frac{L_{j46}}{(\epsilon L_s)_{45}} (n_f/n_-) U_{Af}^2 \quad (9)$$

with $(\epsilon L_s)_{45}$ being the fraction of soft-photon luminosity that is scattered across the jet in units of 10^{45} erg s $^{-1}$. This ratio is independent of radius when $p = 1$ in eq. (2) (provided the soft photon intensity declines as r^2). Nevertheless, enhanced compression during the radiative phase renders it time dependent, as shown in fig. 1. For the parameters adopted in fig. 1 electron cooling is dominated by ERC emission as long as $L_j < 10(\epsilon L_s)$.

3.3. Numerical results

The numerical model presented in Paper I has been extended to include equations (3)-(7). The entire set of equations has then been integrated, starting from r_o where $I_\nu = 0$, and where the front structure is taken to be that of an adiabatic front (see Paper I for a detailed discussion concerning the initial conditions). In the following examples the Lorentz factors of the fluids ahead and behind the front and the rest frame Alfvén 4-velocity have been chosen to be respectively 5, 20, and 10, as in Paper I. A rapid magnetic field dissipation with the same decay constant as in Paper I ($\alpha_b = 0.5$), and a background radiation field with the same intensity have been invoked.

We examine first the dependence of the variability pattern on the thickness of expelled fluid slab, d , in the case in which the maximum injection energy, E_{emax} , is time independent. As shown below, both the shape of the light curve and the spectral evolution depend on d . Quite generally we find that the ejection of slabs of thickness $d \gg r_o$ leads to the production of asymmetric flares with a fast, exponential rise and a much slower, power law decline, as shown in the *bottom right* panel of fig. 2, where a sample light curves of the optically thin emission, computed for different values of d/r_o is exhibited. The decay time and profile in this case are determined predominantly by the decline of the density and magnetic field inside the front due to its transverse expansion. When the expelled slab is sufficiently thin, specifically, when d/r_o is smaller than approximately $(1 - \beta_c)$, β_c being the average front velocity, shock crossing of the fluid slab followed by a large drop of the energy dissipation and consequent particle acceleration rates occurs on a timescale much shorter than the time change of the front parameters due to expansion. As a result, the radiated flux decay on the cooling time scale (provided it is short enough), leading to a roughly symmetric light curve

with exponential rise and decay. The observed duration of the flare in this case is on the order of d/c . An example is shown in the *upper left* panel in fig. 2. Intermediate length outbursts can give rise to light curves that exhibit a fast rise, a plateau and a steep decline, as illustrated in the *upper right* and *bottom left* panels.

Fig. 3 displays light curves at different observing frequencies (10, 10^3 , 10^5 , and 10^6 GHz, with logarithmic energy intervals), produced for $d/r_o = 10^{-2}$, and different values of r_o . As seen, the low frequency flux is delayed, owing to self absorption at the early stages of the outburst. Furthermore, the low frequency emission is strongly depressed when the radius of front formation, r_o , is sufficiently small. In the example depicted in fig. 3 there is essentially no radio emission for r_o smaller than about 10, and very little emission even at millimeter wavelengths for $r_o < 1$. The suppression of the flux at 10^6 GHz seen for $r_o = 10^2$ in the *upper left* panel in fig. 3, is due to our choice of E_o and B_o in eqs. (1) and (2). The total gamma-ray flux is emitted from roughly the same radii as the optically thin synchrotron flux and, therefore, correlations between the gamma-ray and optical/UV emission are expected. The precise relation, however, depends upon the combination of parameters through the radiative feedback and the evolution of the pair cascade, but the time lags should not exceed the flare duration. We emphasize that the gamma-ray flare can either lead or precede the optical/UV emission. As discussed in Paper I, the gamma-ray flux above the initial gamma-spheric radius should also be delayed and, for small enough r_o , will be strongly attenuated by pair production on external photons. Hence, we anticipate some correlated activity of the low-frequency and the hard gamma-ray emission (see further discussion below).

The dependence of flare's properties on p (defined in eq. [2]) is shown in fig. 4, for infinite length outbursts. As expected, increasing p results in a substantially steeper decay of the emitted flux. As illustrated by this example, roughly symmetric flares can be produced essentially for a steep enough magnetic field profile, even in the case of thick slabs. The suppression of the low frequency flux at larger values of p , seen in the figure, is due to the steeper decline of the ratio of synchrotron and Compton cooling rates with time (see eq. [9]). In the case of short length outbursts, the light curve is essentially insensitive to the radial profile of the magnetic field.

Finally, we consider a situation whereby the maximum injection energy evolves with time. We then anticipate the development of the synchrotron flux at frequencies above the initial cutoff frequency, $\nu_{max} = (3eB/4\pi m_e c)E_o$ (cf. eq. [1]), to be governed by the evolution of $E_{emax}(t)$, whereas at lower frequencies the light curves should be highly insensitive to $E_{emax}(t)$, reflecting mainly the evolution of the synchrotron opacity, as in the previous example. This is illustrated in fig. 5, where light curves computed for infinite length outbursts and $b = 1$ in eq. (1) are plotted. As seen, the onset of the flare at high frequencies becomes more delayed and the maximum flux becomes smaller for lower cutoff energies, E_o .

4. Summary and Conclusions

In this paper we considered the time dependent synchrotron emission produced by radiative fronts propagating in a magnetically dominated jet, and examined the relation between the synchrotron and ERC emission. Using a numerical model developed earlier, we analyzed the dependence of the variability pattern on the model parameters, and demonstrated how a change in physical parameters can lead to considerably different temporal behavior. We now summarize our results and conclusions.

Two important parameters determine, in addition to the radial profile of the jet's magnetic field, the shape of the flare and the spectral evolution of the broad-band emission; the thickness of expelled fluid slab, and the radius at which the front is created. Ejection of sufficiently thin slabs leads to the production of

roughly symmetric flares with exponential rise and decay, as occasionally seen in blazars (e.g., Massaro et al. 1996; Urry et al. 1997). The duration of the optically thin flare in this case should be on the order of the light crossing time of the ejected fluid slab, which can be as short as r_g/c , where r_g is the gravitational radius of the putative black hole (cf. Paper I). The low frequency emission is quite generally delayed due to optical depth effects. Such delays provide an important diagnostic of radiatively efficient, inhomogeneous models in general, and are in agreement with the delays (of weeks to months) between high-energy and radio outbursts often observed (Reich et al. 1993; Wehrle et al. 1998), and the ejection of a superluminal blob following a gamma-ray flare (Zhang et al. 1994; Wehrle et al. 1996; Otterbein et al. 1998). The much shorter lags (hours to days) between the peaks of the gamma-ray, UV and optical fluxes, as seen on several occasions (e.g., Edelson et al. 1995; Urry et al. 1997; Wehrle et al., 1998), are also a natural consequence of this model. The precise relation between the optically thin emission in different bands depends on the conditions in the source through the radiative feedback and the evolution of pair cascades inside the front. If, in addition to being thin, the front is formed at a sufficiently small radius, then the low-frequency synchrotron flux will be strongly suppressed by virtue of self absorption, and the gamma-ray flux at energies above the corresponding gamma-spheric energy, will be severely attenuated by pair production on external photons ahead of the front. This implies that i) during such episodes a source may exhibit gamma-ray and UV/optical outbursts followed by little or no activity at low (typically radio-to-submillimeter) frequencies, and ii) in a single object the cutoff energy of the gamma-ray spectrum should be smaller for shorter outbursts, and should be correlated with the lack of activity (or with the amplitude of variations) at long wavelengths. Successful detection of such correlations in a source, particularly ii), will provide a strong support to this model, as such a behavior is not expected in SSC models or other types of inhomogeneous models and is, therefore, distinctive. For a reasonable choice of parameters we estimate the cutoff energy of the gamma-ray spectrum in the powerful blazars (which are likely to be ERC dominated) to lie in the range between a few GeV to a few hundreds GeV. It may be possible to observe it with the next generation gamma-ray telescope or, perhaps, with upcoming ground based experiments.

Intermediate length outbursts can produce synchrotron light curves that exhibit a relatively rapid rise, a plateau and a sharp decay. We argue that the light curves reported by the PKS 2155, 1991 campaign (Urry et al. 1993; Courvoisier et al. 1995) might have been produced by such an event. A rise on a time scale of order a few days followed by a period of about 20 days during which the average flux remained at maximum level is evident (although the flux fluctuated around the maximum level during this period). Unfortunately, there is no data at later times. The faster, small amplitude oscillations may be caused by subsequent formation of smaller fronts, by instabilities, or by inhomogeneities in the upstream flow (which would lead essentially to bifurcation of the front). Furthermore, there is indication (Edelson et al. 1995) that the variation of the radio emission is delayed and has a smaller amplitude, consistent with this model. It is also tempting to relate the difference in temporal behavior seen by the 1991 and 1994 campaigns to the difference in conditions, particularly the length of the outburst, during those two episodes (cf. Georganopoulos & Marscher 1997).

When the thickness of expelled fluid slab largely exceeds the formation radius, which happens when the injection time of the jet by the central engine is much longer than the fluid acceleration time, the resultant light curve will exhibit an exponential rise and a power law decline. If the radial decrement of the jet's magnetic field is not too steep ($p < 2$ in ep. [2]) then the flare will appear asymmetric, with a decay much longer than the rise when viewing the source at small enough angles. At larger viewing angles the shape of the flare may be altered by orientation effects (Eldar & Levinson, in preparation). Such asymmetric flares are atypical to blazars, but are characteristic to GRB afterglows.

In situations where the maximum injection energy increases with time, the onset of outbursts at frequencies above the initial upper cutoff becomes delayed, with longer time lags and smaller peak fluxes at higher frequencies, in contrast to the tendency found in the case of time independent E_{emax} . The gamma-ray light curve should not be affected significantly though (Levinson 1996), in contrast to the evolution predicted by SSC type models. Such events can lead to delayed, lower amplitude variations at optical/UV wavelengths, or even to the lack of apparent variations at these frequencies. Since the evolution of E_{emax} is dictated by the rate of electron acceleration in the front, careful examination of the correlations at short wavelengths can provide important information regarding the acceleration process.

Finally, we note that the inclusion of the SSC process may alter our results somewhat, particularly for parameters typical to fainter sources. The study of SSC flares is left for future work.

I thank Avigdor Eldar for useful discussions, and the anonymous referee for constructive criticism. This research was supported by a grant from the Israeli Science Foundation and by Alon Fellowship.

A. Appendix: Transformation of the electron distribution function

We suppose that the electron distribution is isotropic in the frame of the front, and denote by $n(\mathcal{E}, \mu)$ and $n'[\mathcal{E}'(\mathcal{E}, \mu)]$ the differential number density per unit energy per solid angle, as measured in the injection frame and front frame, respectively, where

$$\mathcal{E}'(\mathcal{E}, \mu) = \mathcal{E}\Gamma_c(1 - \beta_e\beta_c\mu); \quad \beta_e = \sqrt{1 - \mathcal{E}^{-2}}. \quad (\text{A1})$$

The relation between the electron distributions in the two frames reads

$$n(\mathcal{E}, \mu) = \left(\frac{\mathcal{E}}{\mathcal{E}'}\right)^2 n'(\mathcal{E}'). \quad (\text{A2})$$

Averaging over angles yields

$$n(\mathcal{E}) = \int_{-1}^1 n(\mathcal{E}, \mu) d\mu = \frac{\mathcal{E}}{\Gamma_c\beta_c\beta_e} \int_{\mathcal{E}\Gamma_c(1-\beta_e\beta_c)}^{\mathcal{E}\Gamma_c(1+\beta_e\beta_c)} \frac{n'(\mathcal{E}')}{\mathcal{E}'^2} d\mathcal{E}'. \quad (\text{A3})$$

Taking the derivative with respect to \mathcal{E} of the last equation yields,

$$n'[\mathcal{E}\Gamma_c(1 - \beta_e\beta_c)] = n'[\mathcal{E}\Gamma_c(1 + \beta_e\beta_c)] \frac{(1 - \beta_e\beta_c)^3(\beta_e + \beta_c)}{(1 + \beta_e\beta_c)^3(\beta_e - \beta_c)} + \frac{\Gamma_c^3\beta_c(1 - \beta_e\beta_c)^3}{(\beta_e - \beta_c)} \left\{ (3\beta_e^2 - 1)n(\mathcal{E}) - \beta_e^2 \frac{dn(\mathcal{E})}{d\ln\mathcal{E}} \right\}. \quad (\text{A4})$$

The distribution $n'(\mathcal{E}')$ can be calculated now by recursion using the last equation.

REFERENCES

Aharonian, F. et al. 1998, A&A, submitted

Blandford R.D., & Levinson, A. 1995, ApJ, 441, 79 (BL95)

Bloom, S.D., & Marscher, A.P. 1993, in Compton Gamma-Ray Observatory, ed. N. Gehrels (New York: AIP), pp. 578

Brinkmann, W., et al. 1994, A&A, 288, 433

Buckley, H.H. et al. 1996, ApJ, 472, L9

Courvoisier, T.J., et al. 1995, ApJ, 438, 108

Dermer, C., & Schlickheiser, R. 1993, ApJ, 416, 458

Georganopoulos, M., & Marscher P.A. 1997, in Relativistic Jets in AGNs, eds. M. Ostrowski et al., (Krakow: Poligrafia ITS), 313

Levinson, A. 1996, ApJ, 459, 520

Levinson, A. 1998, ApJ, 507, 145 (Paper I)

Levinson, A. & Van Putten, M.V.P. 1997, ApJ, 488, 69

Macomb, D.J., et al. 1995, ApJ, 449, L99

Massaro, E. et al., 1996, A&A, 314, 87

Mastichiadis, A., & Kirk, J.G. 1997, A&A, 320, 19

Mattox, J., et al. 1997, ApJ, 476, 692

Otterbein, K. et al. 1998, A&A, 334, 489

Reich, W., et al. 1993, A&A, 273, 65

Romanova, M.M., & Lovelace, R.V.E. 1997, ApJ, 475, 97

Roelling, T.L., Werner, M.W., Becklin, E., & Impey C.D. 1986, ApJ, 304, 646

Rybicki, G. & Lightman, A.P. 1979, Radiation Processes in Plasmas (New York: Wiley)

Stevens, J.A., et al. 1994, ApJ, 437, 91

Ulrich, M., Maraschi, L., & Urry, M.C. 1997, ARA&A, 35, 445

Urry, C.M., et al. 1993, ApJ, 411, 614

Urry, C.M., et al. 1997, ApJ, 486, 799

Wagner, S. 1997, in Relativistic Jets in AGNs, eds. M. Ostrowski et al., (Krakow: Poligrafia ITS), 208

Wehrle, A.R., et al. 1998, ApJ, 497, 178

Zhang, Y.F., et al. 1994, ApJ, 432, 91

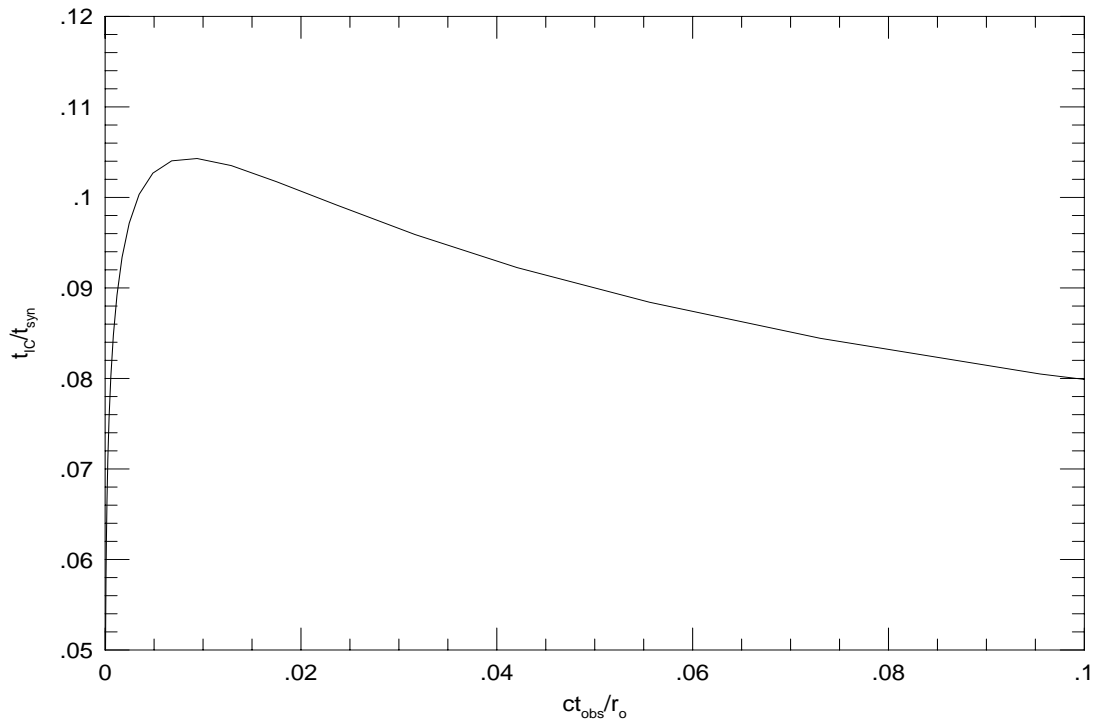


Fig. 1.— Ratio of inverse Compton to synchrotron cooling times as a function of observer time, for $r_{o16} = 1$, $(\epsilon L_s)_{45} = 1$, and $L_{j46} = 1$.

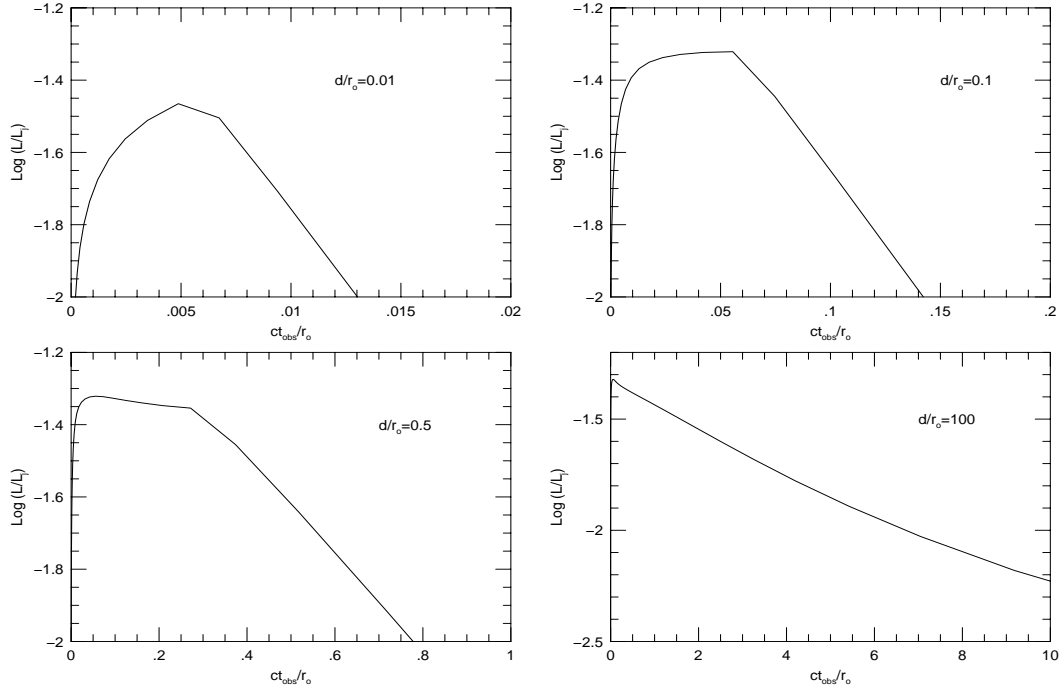


Fig. 2.— Synchrotron light curves at 10^6 GHz produced by the model, for $L_{j46} = 1$, $(\epsilon L_s)_{45} = 1$, $r_{o16} = 1$, and different values of d/r_o (as indicated). Shown is the log of the apparent luminosity (in units of L_j) radiated into a logarithmic frequency interval centered at the corresponding frequency, as a function of observing time.

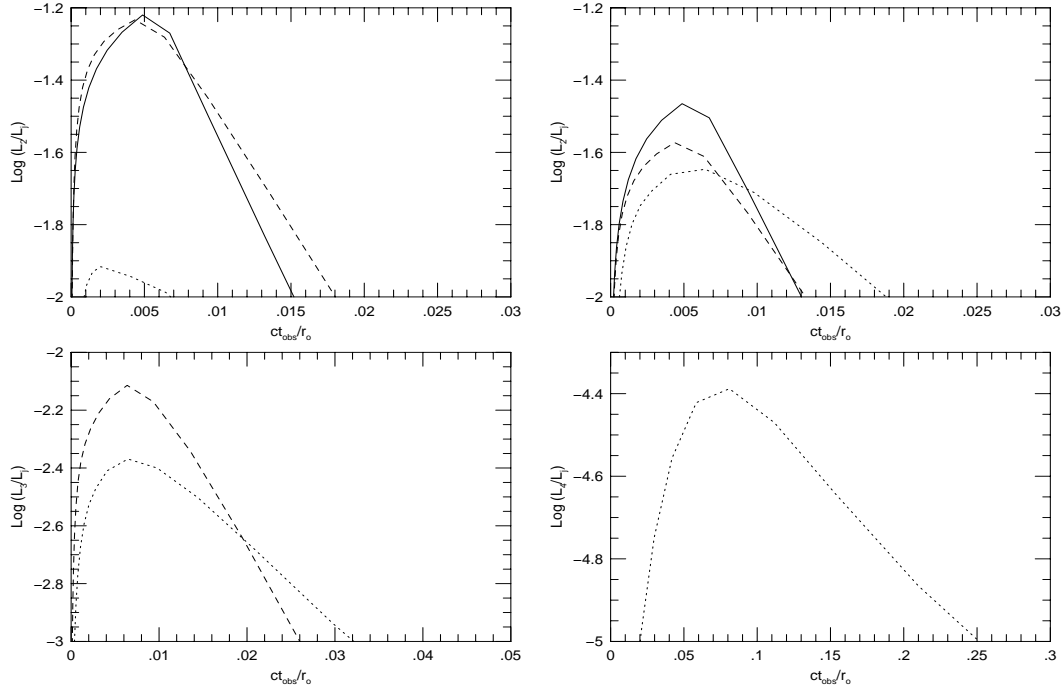


Fig. 3.— Synchrotron light curves at 10^6 GHz (upper left), 10^5 GHz (upper right), 10^3 GHz (bottom left), and 10 GHz (bottom right), produced using $L_{j46} = 1$, $(\epsilon L_s)_{45} = 1$, $d/r_o = 10^{-2}$, and different values of r_o ; $r_{o16} = 1$ (solid line), $r_{o16} = 10$ (dashed line), and $r_{o16} = 10^2$ (dotted line).

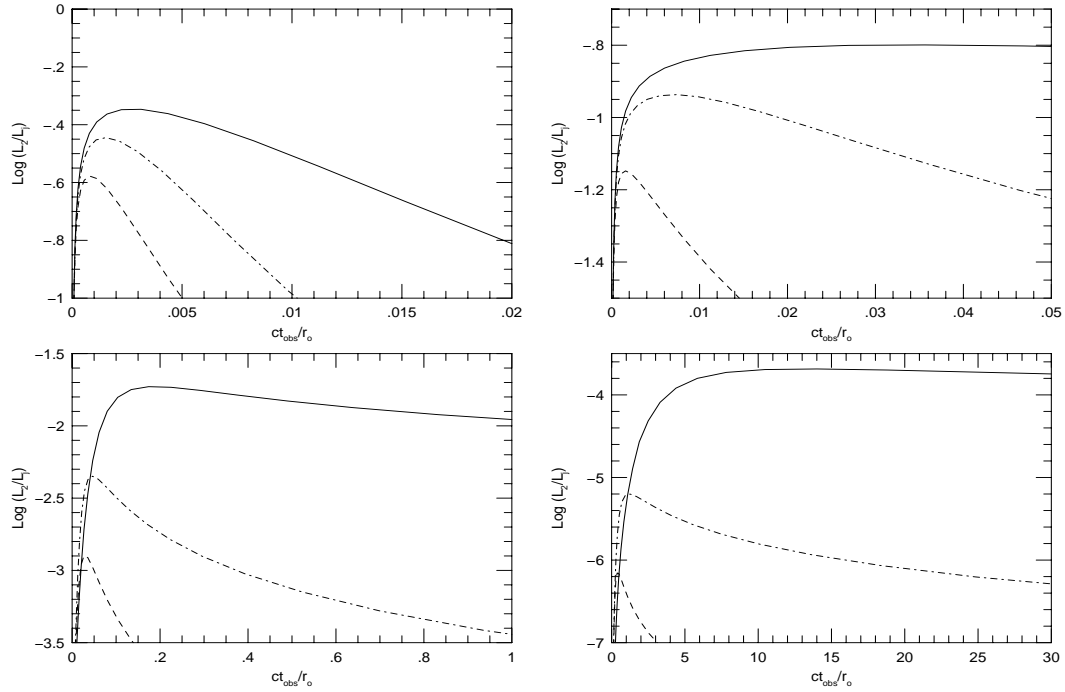


Fig. 4.— Same as fig. 3, but for $L_{j46} = 1$, $(\epsilon L_s)_{45} = 0.1$, $r_{o16} = 1$, $p = 1$ (solid line), $p = 1.5$ (dotted dashed line) and $p = 2$ (dashed line).

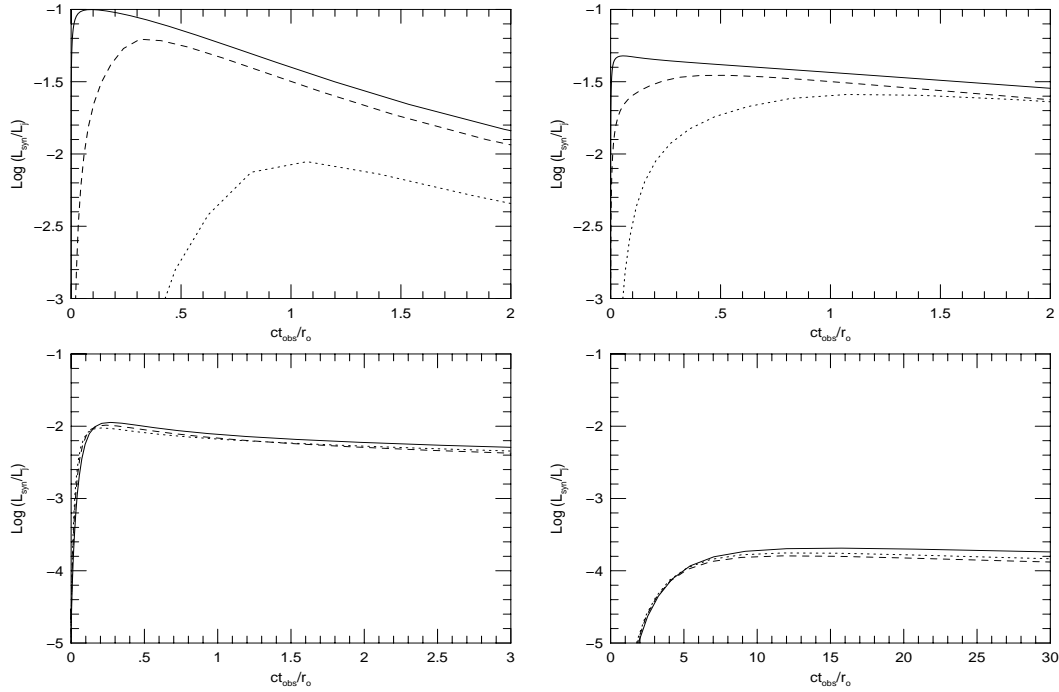


Fig. 5.— Same as fig. 4 with $p = 1$, but for injected electron spectrum with a maximum cutoff energy that varies according to eq. (1), with $b = 1$, $E_o/(m_e c^2) = 5 \times 10^2$ (dotted line), 2×10^3 (dashed line), and 10^5 (solid line).